

# Automatic seismic swarm analyzer system based on template matching algorithms and *Master-Cluster* relative location methods

Eduardo Andrés Díaz Suárez<sup>1</sup> (eadiaz@mitma.es, @EADSuarez)  
Itahiza Dominguez Cerdeña<sup>1</sup> (ifdominguez@mitma.es, @ita\_dc)  
Carmen del Fresno<sup>2</sup> (cdelfresno@mitma.es)

<sup>1</sup>Instituto Geográfico Nacional, Santa Cruz de Tenerife, ES

<sup>2</sup>Instituto Geográfico Nacional, Madrid, ES

This manuscript has been submitted for publication in **Geophysical Journal International** and is undergoing peer-review. Please note that the manuscript has not been formally accepted for publication. Subsequent versions of this manuscript may have slightly different content. If accepted, the final version of this manuscript will be available via the Peer-review Publication DOI link on this webpage. Please feel free to contact the authors; We welcome feedback.

# **Automatic seismic swarm analyzer system based on template matching algorithms and *Master-Cluster* relative location methods**

Eduardo Andrés Díaz Suárez<sup>1</sup>, Itahiza Dominguez Cerdeña<sup>1</sup>, Carmen del Fresno<sup>2</sup>

<sup>1</sup> *Centro Geofísico de Canarias, Instituto Geográfico Nacional (IGN), España. E-mail: eadiaz@mitma.es*

<sup>2</sup> *Observatorio Geofísico Central, Instituto Geográfico Nacional (IGN), España*

Received –; in original form –

## **SUMMARY**

Seismic swarms may have periods of intense activity with a high number of earthquakes per hour, with overlapping events and/or low signal-to-noise ratio seismic records. During these intervals, the manual characterization of the activity can become very complex to perform by seismic or volcanic observatories, resulting in inhomogeneous seismic catalogs. In order to tackle this problem, we have developed a set of automatic algorithms capable of detecting earthquakes, picking their P and S arrivals and locating the events with absolute and relative methodologies. Detections are performed over the filtered seismic energy while phase picking is based in the correlation of new events with a set of previous well-characterized templates. Absolute locations are computed using traditional algorithms as Hypoellipse and for relative locations we introduce a novel technique *Master-Cluster*, which is a hybrid between the double differences and the master event.

The algorithms have been tested on real data of two series corresponding to two different tectonic regimes: the volcanic pre-eruptive swarm of El Hierro, Spain (2011) and the tectonic seismic series of Torreperogil, Spain (2012-2013). Both data sets are considerably different in terms of epicentral distances and distribution of the network varying from stations very close to the activity at El Hierro (5-20 km) to regional distances in the case of Torreperogil (10-180km).

The templates were taken as a partial dataset of 3 600 (El Hierro) and 800 (Torreperogil) re-located earthquakes from the manual regional catalog. Based on these datasets, the algorithm was able to improve the number of events by a factor of 6 in El Hierro and 10 in Torreperogil, producing a seismic catalog between 3 and 4.5 times larger than the manually obtained one. An additional test was performed with the smaller earthquakes (local magnitude < 1.5) which were not included in the set of templates, resulting not only in a good factor of success –larger than 65% of events were retrieved in both series– but also an enhancement in their automatic locations was observed with a more clustered seismicity than the previous catalog.

**Key words:** Time-series analysis, Computational Seismology, Statistical Seismology

## 1 INTRODUCTION

In the last two decades, there has been a significant leap in the seismic monitoring networks throughout the world (Mignan & Chouliaras 2014; Dondin et al. 2019). Lower cost and optimization of real time data transmission systems and instrumentation (Jourdan & de Weck 2004; Werner-Allen et al. 2008; Lopes Pereira et al. 2014) has allowed the densification of the seismic monitoring networks, and the volume of data generated has increased exponentially. This has led to a substantial improvement in real-time seismic monitoring, seismic hazards mapping and knowledge of the local and regional dynamics of seismically active zones (Benz 2017; Bianchi et al. 2018; Bent et al. 2018). As a consequence, the capability to characterize and analyze the low magnitude seismicity has improved and established as a new focus of study (Cesca & Grigoli 2015; Grigoli et al. 2017). During seismic swarms, there are considerably more low magnitude earthquakes than high magnitude earthquakes (Gutenberg & Richter 1944). Therefore, real-time manual analysis of seismic swarms can become an impossible task with dramatic consequences: First, low completeness seismic catalogs may lead to a misinterpretation of the ongoing phenomenon. Second, late warning to the population of the hazard associated to seismic swarms such as high magnitude earthquakes or volcanic eruptions that could be forecasted by precursory seismic activity.

A large amount of techniques for earthquake detection and phase picking have been developed

19 over the years. The first approximation for automatic detection was introduced by [Allen \(1982\)](#),  
20 comparing variations in ratios between long-term and short-term energy windows, known as the  
21 classical STA/LTA. Subsequently, several methodologies were proposed, such as the application a  
22 STA/LTA to signal envelopes ([Baer & Kradolfer 1987](#)), or more complex studies of signal Gaus-  
23 sianity variations as a function of high order statistical parameters such as kurtosis and skewness  
24 ([Saragiotis et al. 2002](#); [Küperkoch et al. 2010](#)). In recent years, several techniques have been devel-  
25 oped based on the use of reference templates for earthquake characterization and, in particular, mi-  
26 croseismicity. Usually, the templates selected are waveforms manually analyzed by a seismologist  
27 that faithfully represent a group or the totality of the seismicity. These methods can be separated  
28 into two main groups: cross-correlation techniques ([Chamberlain et al. 2017](#); [Vuan et al. 2018](#);  
29 [Chamberlain et al. 2020](#); [Beaucé et al. 2017](#); [Senobari et al. 2019](#)) and neural network techniques  
30 ([Zhu & Beroza 2018](#); [Perol et al. 2018](#); [Liu et al. 2020](#)). These methodologies are based on phase  
31 picking, however, there are several alternative techniques that perform the analysis of seismic sig-  
32 nals based on the 'brightness' function of signals from a network of seismic stations ([Kao & Shan](#)  
33 [2004](#), [2007](#); [Journeau et al. 2020](#)). Most methodologies provide a solution for the simultaneous  
34 detection, characterization and localization of seismicity but with a large computational cost and,  
35 generally, without a phase characterization.

36 In this paper, we introduce a new automatic seismic swarm analysis system tested on two dif-  
37 ferent seismic series. The objective of this system is to simplify and enhance the analysis carried  
38 out in seismic and volcanic observatories by performing the detection, phasing and earthquake  
39 localization. The detection is performed using the classical STA/LTA algorithm applied over the  
40 spectrograms of the seismic signals of our network. Afterwards, a matched-filtering algorithm per-  
41 forms the phase picking, using earthquakes manually analyzed as templates. Once the phases are  
42 obtained, direct inversion is performed and the location is obtained using Hypoellipse ([Lahr 1999](#)).  
43 At the same time, using the methodologies of double differences, the algorithm improves the lo-  
44 calization relocating the new detected earthquakes employing the template locations as multiple  
45 master events. The pipeline has been designed to allow full parallelization in order to optimize the  
46 computational time consumption.

The algorithm has been tested on two different data sets: Pre-eruptive unrest phase of El Hierro eruption (2011) and Torreperogil seismic swarm (2012-2013). These series represent two good examples for testing the algorithm developed thanks to the different network distances regime: local for the pre-eruptive phase of El Hierro and regional for the Torreperogil crisis. The algorithm has been developed in Python Language using Numpy, Obspy, Scipy and Multiprocessing (Harris et al. 2020; Beyreuther et al. 2010; Virtanen et al. 2020; McKerns et al. 2012).

## 2 METHODOLOGY

Our main goal is to optimize the automatic information obtained from the analysis during dense seismic swarms such as number of earthquakes and their hypocentral location in order to decrease the manual workload of the observatories. The algorithm is structured in three main modules: Detection, Phase Picking and Localization. Each module can be used independent from each other.

### 2.1 Earthquake Detection

Earthquakes recorded at epicentral distances closer than 200-300 km are usually characterized by a narrow-line energy distribution in frequencies between 0 and 25 Hz, which can be taken as an advantage to identify them with low uncertainty. Therefore, a STA/LTA is applied over seismic energy trace.

Raw data is filtered with a butter-worth bandpass filter to suppress ambient noises, natural features as high frequency antropoc activity or low frequency natural signals: tidal waves, tectonic tides, etc. Then the energy of the signal  $x[i]$  in the time window  $w$  is obtained as:

$$Energy = \sum_{j=0}^{N-w} \left[ \frac{1}{w} \sum_{i=j}^{j+w} x[i] \right]^2 \quad (1)$$

The algorithm associates individual detections in different stations when they coincide in time. We assume that the hypocentral centroid of the catalog earthquakes has a similar location to the new detections. Therefore, the timelags between seismic stations are obtained from the previous catalog. When a match occurs at a minimum number of stations, the detection is classified as a potential earthquake.

The STA/LTA algorithm is very popular in the literature due to its simplicity and Robustness. However, determine the optimum window length of the STA and LTA and the threshold-detection, could be overwhelming. Those parameters depend on diverse features as the noise levels, the sensibility of our seismometers or the filter used in data processing. Therefore, an optimum calibration is obtained using a few hours of manually picked data as reference.

All the permutations are evaluated for a range of window lengths and thresholds, choosing the best solution as the one that obtains the best perform for two binary classifiers (Murphy 2012),  $R$  and  $F_1$ , in a certain data set. The traces selected to calibrate the detectors have to fairly reproduce the main characteristics of the seismic activity to analyze. Defining  $t_p$  as true positives,  $f_n$  as false negatives,  $f_p$  as false positives and  $N_d$  manually detected earthquakes, the two parameters to optimize are:

$$R = \frac{t_p - f_n}{N_d} \quad (2)$$

And the second one, the  $F_1$ -Score:

$$F_1 = \frac{t_p}{t_p + \frac{1}{2}(f_p + f_n)} \quad (3)$$

Both parameters weight the true positives above all the detections. While  $R$  penalizes the false negatives above all the detections, as an absolute ratio,  $F_1$  measures the relation between the true positives and the false performance of the detection, as a relative ratio. Once the detector has been calibrated, the final parameters are tested in a new manually detected trace, in order to check the final set of parameter combinations.

## 2.2 P and S Phase Picking

During seismic swarms, earthquakes are usually clustered in small regions having similar focal mechanisms. Ray tracing and radiation pattern may be almost identical for several events, their waveforms may be highly correlated and earthquakes can be classified in a small number of families (Okada et al. 1981). Cross correlation and template matching techniques, have been successfully applied previously to tectonic and volcanotectonic seismicity (e.g., Okada et al. 1981; Umakoshi et al. 2008; Carmona et al. 2010; Domínguez Cerdeña et al. 2011; Chamberlain et al.

2020). Therefore the phase-picking is carried out by seismic waveform cross correlation in different stages.

### TEMPLATE CLASSIFICATION

Our algorithm works using previous analyzed earthquakes, preferably well-characterized as a template set of data (i.e., catalog earthquake with magnitude above certain value or a minimum number of phases / stations).

A first step is to classify the template earthquakes into different families by waveform cross-correlation. This classification have been used successfully for the seismicity of many volcanoes (Okada et al. 1981; Lahr et al. 1994; Stephens & Chouet 2001). Events from a single family should produce very similar focal mechanism and be grouped within a small volume.

To classify each cluster, we calculate the normalized full wave cross correlation between all templates at each station. A correlation matrix  $cc_{i,j}$  is obtained, where  $i$  and  $j$  are the template indices. The correlation matrix in time space can be defined as signals convolution:

$$cc_{i,j}(\tau) = \frac{\sum_{t=0}^N x_i(t) \otimes x_j(t + \tau)}{\sqrt{\sum_{t=0}^N x_i^2(t) \cdot \sum_{t=0}^N x_j^2(t + \tau)}} \quad (4)$$

where  $x_i(t)$  and  $x_j(t + \tau)$  are demeaned. The cross correlation matrix is obtained for each station used. Those matrices are added and normalized to one matrix which stores the information of the addition of each cross-correlation per event. Setting a threshold level for the normalized cross correlation coefficient (NCCC), templates are associated in families applying hierarchic analysis (e.g., Domínguez Cerdeña et al. 2011).

The phase picking is performed by cross correlation between the detected and the templates. For each earthquake detection, the algorithm segments and filters the data between two frequencies,  $f_{min}$  and  $f_{max}$ . The phase picking is developed in two steps, which will determine the quality of the picking.

121 *Robust Phases*

122 *Robust Phases* are obtained by cross correlation of the full waveform which includes P, S and  
 123 surface wave data. We correlate each  $i$ -event detected with all the templates, in each  $k$ -station.  
 124 Those pairs detection-template with NCCC that exceeds a threshold, are employed to calculate the  
 125 arrival time, for P and S wave, as a weighted average. The cross-correlation coefficients used as  
 126 weights are renormalized as Got et al. (1994):

$$127 \quad cc_{i,j}^r = \sqrt{\frac{\frac{cc_{i,j}}{1-cc_{i,j}^2}}{cc_{max}^2}}{\frac{cc_{max}^2}{1-cc_{max}^2}}}, \quad (5)$$

128 where  $c_{i,j}$  are the NCCC obtained by Eq. (4) between  $j$ -template and the  $i$ -event,  $c_{max}$  the  
 129 larger  $c_{i,j}$  and  $cc_{i,j}^r$  the renormalized cross correlation coefficient (RNCCC). Then, P and S *Robust*  
 130 *Phases* are determined for the  $i$ -event detected in the  $k$ -station.

131 Time lags and NCCCs between this earthquake and each of the templates are also stored. In  
 132 consequence, after this step, we can classify each detected event and assign it to the family (or the  
 133 group of families) with highest correlation.

134 *Fine Phases*

135 Calculation of *Fine Phases* is the second step in the phase picking process. The algorithm segments  
 136 the P and S waveform of the templates to correlate them, separately. Subsequently, the P and S  
 137 *Robust Phases* can be refined by correlate them with the P and S templates.

138 The S phases are correlated in horizontal components and the P phase in the vertical ones. The  
 139 detection window length to correlate the templates is predefined, as well as the threshold to take  
 140 them to account to refine the picks. Following the same procedure, the NCCCs are renormalized  
 141 to the maximum NCCC obtained using Eq. (5) for each phase. If the templates correlates above  
 142 the threshold, *Fine Phases* are obtained as a weighted-average.



143 *Schedule*

144 The algorithm computes the phase picking through all the data available using initial parameters set  
 145 by the user. It considers a successfully picked earthquake when phases are obtained in a minimum  
 146 number of stations.

147 We have set this minimum to 3, therefore, when that condition is met, the detected earthquake  
 148 is ready to be located and the phase picking process will be set as finished. Phase picking module  
 149 is schedule to start working in a main branch and, if the conditions are not fulfilled, it continues  
 150 working in an alternative branch with lower thresholds.

151 Main branch tries to pick P and S phases by full wave cross correlation as has been described  
 152 before. Regional earthquakes (at larger distances than 80 km) may increase the difference between  
 153 P and S arrivals and decrease the NCCC. Therefore, for regional stations (distances higher than  
 154 80 km from the epicenter), the *Robust Phases* are obtained as *Fine Phases* procedure but with  
 155 slightly variations. To determine the P and S arrival time to segment the waveform, we calculate  
 156 the theoretical arrival time,  $t_{i,k}^m$ :

$$157 \quad t_{teo,k}^m = t_{det,k'}^m + t_k^m - t_{k'}^m, \quad (6)$$

158 where  $t_{det,k'}^m$  is the detection time in the nearest station  $k'$  to the seismicity for the  $m$ -wave (P  
 159 or S wave) and,  $t_k^m - t_{k'}^m$  is the theoretical arrival difference between the nearest station  $k'$ , and  
 160 the regional station  $k$ . Then, the P and S waveforms are cross correlated with all the templates as  
 161 *Fine Phases* process. Finally, if *Robust Phases* are obtained, the algorithm tries to estimate *Fine*  
 162 *Phases*.

163 **2.3 Localization and Master-Cluster Method**

164 The hypocentral location is computed using Hypoellipse (Lahr 1999). A weight is assigned to the  
 165 phases depending on which procedure have been applied to obtain them: we have used for *Fine*  
 166 *Phases* the highest value (0), and second highest (1) for *Robust Phases*.

167 Classical techniques like this are the first approach to the location solution, however, they  
 168 may have multiple sources of error when dealing with low magnitude events and can lead to

169 large error ellipses. Results may show a strong dependence on the velocity models, the number  
 170 of phases and the network azimuthal coverage, giving large error ellipses. An example where these  
 171 methodologies could have misled to a low quality hypocentral location, could be a volcanic island  
 172 where the aperture of the seismic network is smaller than the earthquakes depth and the unknown  
 173 velocity model is far from the commonly used plane parallel model. For this reason, we propose  
 174 to complete the analysis using a relative relocation of the data in our methodology.

175 Relative location techniques allow to obtain hypocentral locations with higher precision than  
 176 the traditional methods. We have developed the new *Master-Cluster* method, which is midpoint be-  
 177 tween two well-known relocation methods, the double-difference (Waldhauser & Ellsworth 2000)  
 178 and master event (Ito 1985). The locations of our templates are known (obtained by classical or  
 179 relative methods). Those locations can be considered as multiple master events if they correlate  
 180 with our problem earthquakes. In other words, the double-difference technique can be applied to  
 181 locate or relocate each problem earthquake but giving a fix location for the templates used. Then,  
 182 the time residuals to minimize  $dr_k^{ij}$  between the  $i$ -event and the  $j$ -template for a  $k$ -station can  
 183 be expressed as:

$$184 \quad dr_k^{ij} = (t_k^i - t_k^j)^{teo} - (t_k^i - t_k^j)^{cal} = \frac{\partial t_k^i}{\partial x} \Delta x^i \quad (7)$$

185 where  $(t_k^i - t_k^j)^{teo}$  corresponds to the theoretical time differences between the templates noted  
 186 as  $j$ , and the  $i$  problem earthquake for an observed phase in a  $k$  station. The term  $(t_k^i - t_k^j)^{cal}$  are  
 187 the cross correlation time lag between the templates and the earthquake to relocate for an observed  
 188 phase at the  $k$  station. The model is introduced in the equation as a partial derivative,  $\partial t_k^i / \partial x$ , which  
 189 contains all the information of angles and velocity layers. Finally, the  $\Delta x^i$  are the temporal and  
 190 spatial corrections to apply to the original location of our earthquake and the RNCCC are used as  
 191 weights in our system of equations

### 192 *Error estimation*

193 Since the relocation process is not a linear method, the error estimation has to be obtained apply-  
 194 ing other techniques. We chose the bootstrap analysis (Efron 1982) which has been successfully  
 195 applied in other studies (e.g., Domínguez Cerdeña et al. 2014; Trugman & Shearer 2017). The ap-

plication of the bootstrap method consists in a statistical resampling of the relocation method, done  $N$  times, and adding or subtracting randomly the residuals obtained for Eq. (7) to cross correlation timelag  $(t_k^i - t_k^j)^{cal}$ . For each earthquake, an  $N$ -size distribution is obtained. As the distribution could have a strong bias or not be correctly described by a normal distribution, other authors (Leys et al. 2013) introduce the median absolute deviation as an error estimator.

$$err(x) = Median(|x_i - Median(x)|), \quad (8)$$

where  $x$ , corresponds to any of the hypocentral coordinates. The robustness of this nonparametric estimator, avoids the standard deviation problems as biases or skewness (Mammen 1992; Maronna 2011; Hesterberg et al. 2005, e.g.).

### Workflow

In order to solve the Eq. (7) by an iterative approach an initial location is needed. The inverse of  $\partial t_k^i / \partial x$  can be calculated using singular value decomposition and the equations system is weighted with the cross correlation renormalized coefficient (Eq. (5)).

As an initial solution, we could use the Hypoellipse results for each earthquake, however, due to the low quality of some phases, the hypocenter results are sometimes too far from the templates location. In order to solve this fact, our algorithm can consider whether the centroid of the best correlated templates as an initial solution, weighted with the cross correlation using a normalized coefficient, or just the location of the template with the maximum NCCC.

Furthermore, different quality controls has to be applied during the iterative process. First, a residual control is applied. After the first iteration, all the residuals of all the equations introduced to our system are evaluated. If these time residuals are higher than a time threshold, this equations are subtracted from the system. If the remaining number of equations are under 5, the subtraction is cancelled and the iteration continues. Second, if the spatial corrections are above certain distance threshold, the iteration stops and tries to find the corrections using an alternative initial location. Finally, if the minimization raises an r-squared value higher than 0.999, the iteration is finished and the new location is stored. Otherwise, if the system does not converge or after a certain number of iterations, the workflow finishes.

## 2.4 Parallelization and Data Storage

Within our methodology we have sectioned each part as independent modules. We consider the possibility that in the future different more sophisticated algorithms may be incorporated for detection, phase picking or localization, therefore, we have proposed the code so that each module can be used separately.

We took advantage of the modular structure proposed to code and parallelize the analysis of seismic swarms in the simplest and most optimal way. For this purpose, we have separated the parallelization into two blocks: On the one hand, detection and on the other hand, phase picking and localization.

Detection is performed between two timestamps in all the selected stations. Therefore, the parallelization could be performed between multiple pairs of timestamps (in our case, hours) at the same time. Moreover, once the detections are obtained, phase picking and localization are performed. Since our methodology analyzes each event independently, we can classify the parallelization of the process as "embarrassing parallel" where in each CPU thread the analysis, phase picking localization and relocalization, are performed.

For each event, an individual JSON file is generated including the obtained phases (Robust and/or Fine), the time differentials of the cross-correlation and the cross-correlation coefficient. In addition, a text file is generated where the hypocentral parameters and the origin time obtained by Hypoellipse and by the *Master-Cluster* method are stored with the corresponding errors.

## 3 DATA

Two data sets have been used to test the methodology described. These data sets correspond to a couple of dense seismic swarms monitored by [Instituto Geografico Nacional, Spain \(1999\)](#), (IGN). In both cases there is a lack of low magnitude events in the catalog. It is known that the manual analysis of these series left behind a large number of earthquakes and the automatic processes which dealt with the data on real time had been overloaded. That were not analysed for various reasons, such as the difficulty of identifying phases and the impossibility to manually analyze all data during dense periods of the seismic series.

**Table 1.** Ground velocity model used for El Hierro and Torreperogil seismic series.

El Hierro			Torreperogil		
Depth [km]	Vp [km/s]	Vp/Vs	Depth [km]	Vp [km/s]	Vp/Vs
0	4.2	1.78	0	6.1	1.75
4	6.3	1.78	11	6.4	1.75
12	7	1.78	24	6.9	1.75
18	8	1.78	31	8	1.75

250 The first data set includes the seismic series that preceded the submarine eruption of Tagoro  
 251 Volcano in the South of El Hierro (Figure 1a), Canary Islands, Spain. The series started on 19<sup>th</sup> of  
 252 July 2011 in the center of the island and migrated southern towards the sea where the eruptive vent  
 253 opened on the 10<sup>th</sup> of October 2011 (López et al. 2012; Domínguez Cerdeña et al. 2014; Sainz-  
 254 Maza Aparicio et al. 2014; Meletlidis et al. 2015). This spatial evolution of the seismicity (Fig. 1c)  
 255 is of great interest to test the designed algorithm. For the analysis, we have used all the seismic  
 256 stations of the IGN network on the island (Fig. 1d). An extensive description of the evolution and  
 257 successive deployment of the seismic network (Fig. 1b) can be found in the literature (López et al.  
 258 2012; Domínguez Cerdeña et al. 2014).

259 On the other hand, we have chosen another series occurred in the South of the Iberian Peninsula  
 260 with a purely tectonic origin, the Torreperogil seismic swarm (Fig. 2a). The activity started on 10<sup>th</sup>  
 261 of October 2012 and lasted for 6 months till the 25<sup>th</sup> of April 2013 (Fig. 2c). We have used data  
 262 from stations of the IGN network in the analysis (Fig. 2a and d). As in the previous data set, the  
 263 seismic network where not very dense at the beginning of the series (Fig. 1b), however, four more  
 264 stations were deployed by late November when seismicity started to increase. A detailed analysis  
 265 of the characteristics of this series can be found in Cantavella et al. (2013).

266 As long as the IGN catalog locations have been obtained with a different algorithm (Locsat),  
 267 we have considered its manually picked arrivals and relocated the events using Hypoellipse in  
 268 order to make them comparable with the solutions of our methodology for both datasets, El Hierro  
 269 (Fig. 1c) and Torreperogil (Fig. 2c). To ensure homogeneity and to be able to compare the results of

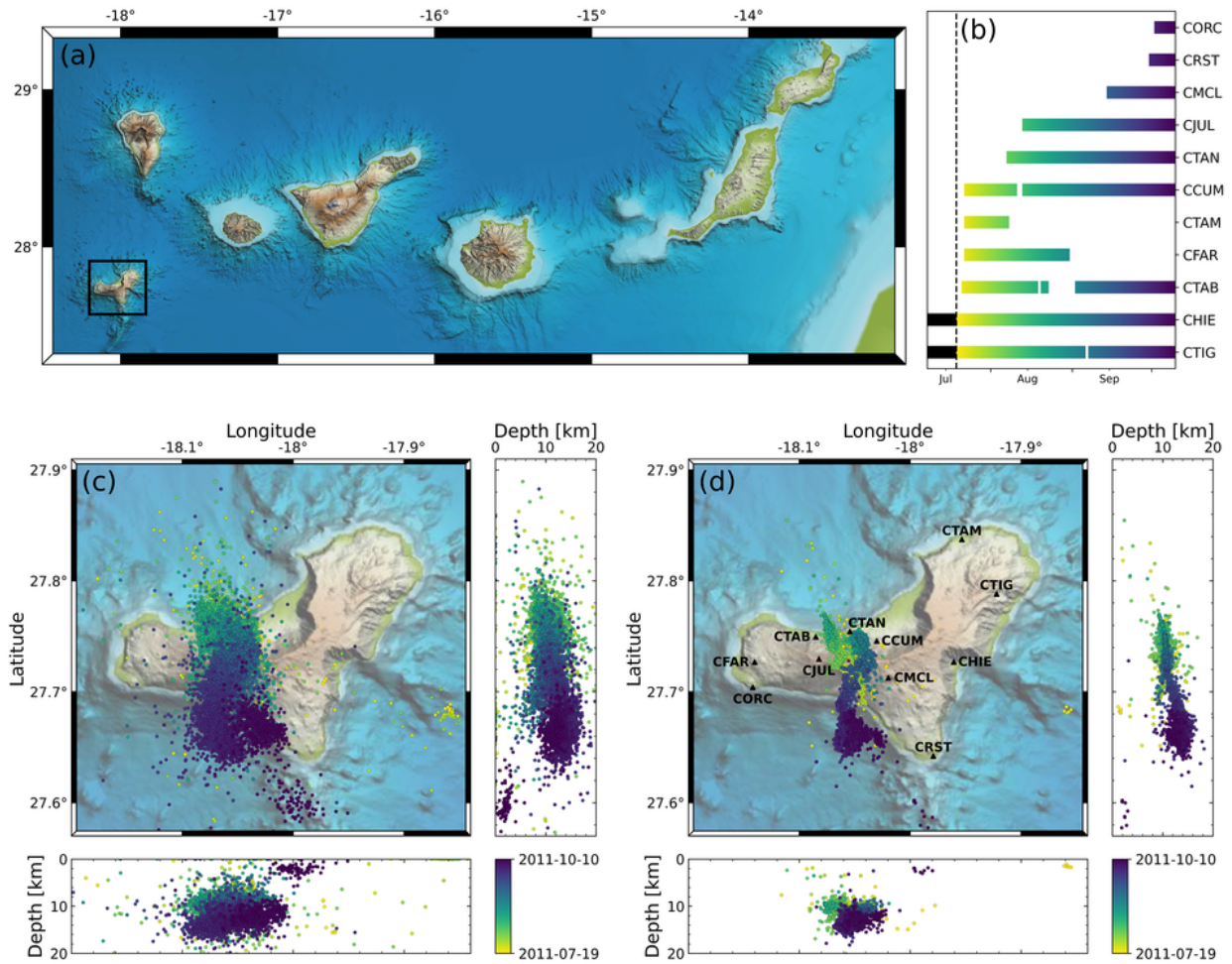


**Figure 1.** Pre-eruptive seismicity of El Hierro eruption (2011). (a) Location of El Hierro highlighted in the Canary Island Archipelago. (b) Evolution of the seismic network indicating the periods of working time for each station. (c) Seismicity of the IGN catalog located by Hypoellipse. Panels show horizontal distribution and vertical projections in latitude and longitude. (d) Seismic templates ( $m \geq 1.5$ ) relocated by HypoDD and local seismic network distribution. The color distribution indicates the time evolution, from 19<sup>th</sup> of July (yellow) to 10<sup>th</sup> of October (dark purple).

270 the program between both data sets, we have used the same criteria to select the templates. Previous  
 271 studies have evaluated the completeness magnitude of the IGN catalog for both swarms, obtaining  
 272 a value of 1.2 mbLg (González 2017) for the pre-eruptive phase of El Hierro and 1.5 mbLg (Yazdi  
 273 et al. 2017) for Torreperogil. Accordingly to this values, we have selected as templates those  
 274 earthquakes from both catalogs that have a magnitude equal to or greater than 1.5 mbLg. In the El  
 275 Hierro catalog, there are a total of 3 601 out of 10 000 earthquakes that satisfy this criterion. For  
 276 Torreperogil, of the 2 500 earthquakes in the seismic catalog, a total of 796 earthquakes fulfill this



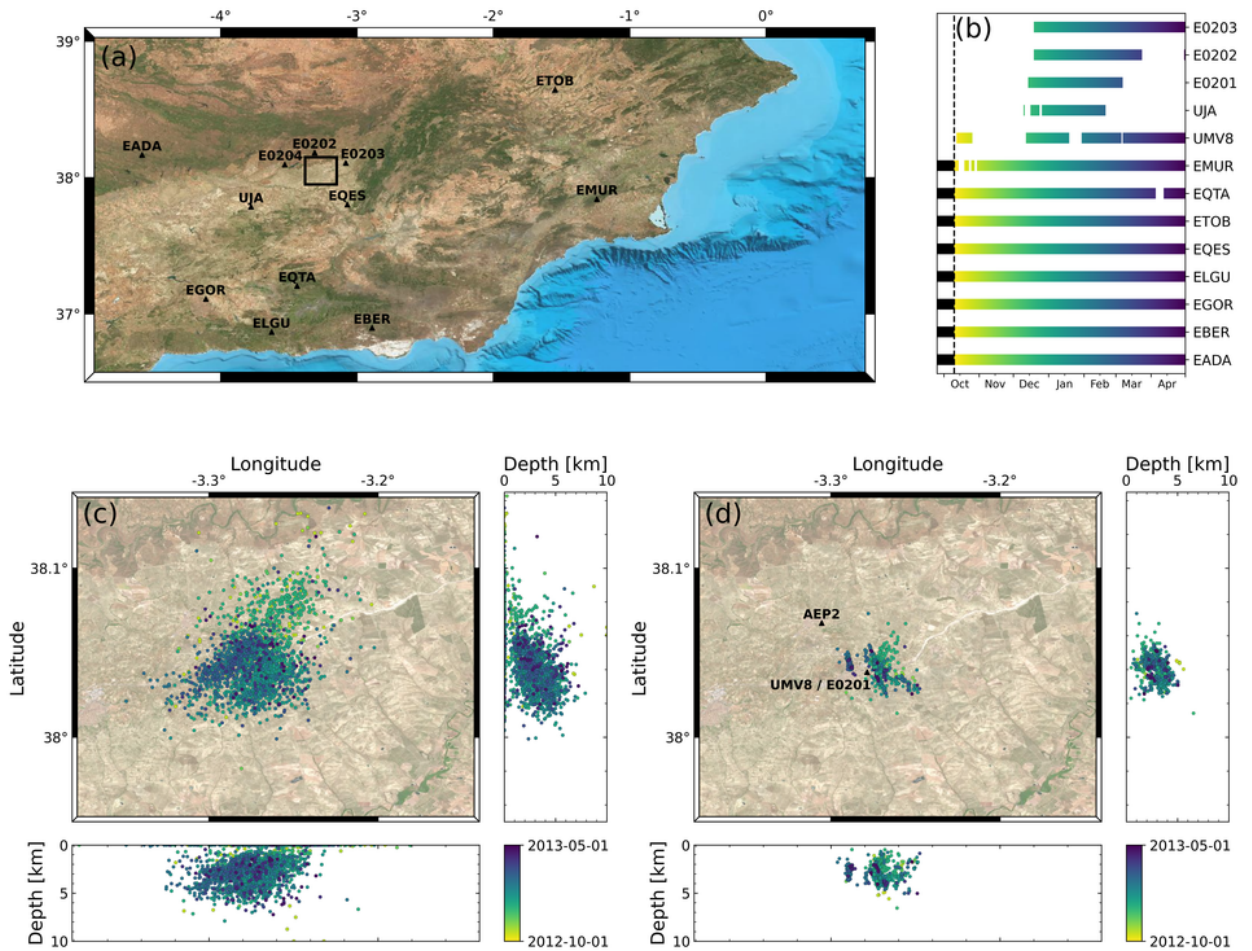


**Figure 2.** Torreperogil seismic swarm 2012-2013. (a) Torreperogil location on the south of the Iberian Peninsula and the seismic network. The black square highlight the Torreperogil area used from now in future maps. (b) Evolution of the seismic network indicating the periods of working time for each station. (c) Seismicity of the IGN catalog located by Hypoellipse. Panels show horizontal distribution and vertical projections in latitude and longitude. (d) Seismic templates ( $m \geq 1.5$ ) relocated by HypoDD and local seismic network distribution. The color distribution indicates the time evolution, from 1<sup>st</sup> of October of 2012 (yellow) to 1<sup>st</sup> of May of 2013 (dark purple).

277 criterion. Both template set have been relocalized using HypoDD (Fig. 1d, Fig. 2d) and considering  
 278 the velocity models (Table 1).

279 Though both seismic swarms have been widely studied due to their geological and geody-  
 280 namical interest (Meletlidis et al. 2015; Sainz-Maza Aparicio et al. 2014; Sánchez-Gómez et al.  
 281 2014; Peláez et al. 2013; Pedrera et al. 2013), a further analysis on the continuous waveform in  
 282 order to detect and locate microseismicity and enhance the seismic catalog has not been done yet.

283 Therefore, the application of our methodology to the swarms will be useful both for testing the  
284 algorithms and also for improving the existing seismic catalogs.

## 285 4 APPLICATION SETTINGS AND RESULTS

286 Although the algorithms has been developed for automatic operation, certain parameters need to be  
287 adjusted and calibrated in order to obtain optimal results. In this section we present the parameters  
288 used for the analysis of the two test data sets and the results obtained.

### 289 4.1 El Hierro

290 The detector has been calibrated using thoroughly manually revised hours. These intervals corre-  
291 spond to three different states of the activity: an hour without earthquakes, a noisy hour with some  
292 earthquakes and an hour with more than a hundred earthquakes. The best performance have been  
293 obtained for a 3 s of STA window, 11 s for LTA window, a trigger ratio of 2.7 and a bandpass  
294 butter-worth filter between 6 and 16 Hz. Values obtained for  $R$  and  $F_1$ , Eq. 2 and 3, are a  $R = 0.77$   
295 and  $F_1 = 0.88$  respectively. This detection parameters were selected after testing the detector to  
296 a set manually revised hours of the swarm and obtaining an  $R = 0.79$  and  $F_1 = 0.89$ , which  
297 corroborate the calibration reliability.

298 The resulting number of detections as potential earthquakes was 40 330. Figure 3a, shows the  
299 evolution of number of earthquakes per day detected by our method (pink bars) and the 10 010  
300 earthquakes registered in the IGN catalog (gray line). Both records show similar trends at the  
301 beginning of the crisis but an outstanding difference between them in late July and during the days  
302 before the eruption onset (October 10<sup>th</sup>).

303 Each detection has been analyzed by applying the phase picking method described in Sec. 2.2.  
304 The seismic stations used for this swarm are located at similar distances from the hypocenters in a  
305 regional configuration, therefore, differences between P-wave and S-wave arrivals are similar for  
306 each station, approximately 2 seconds. Assuming this, we have segmented the templates of all the  
307 stations using the same time length: 2 seconds before the P-wave arrival and 5 seconds after. If the



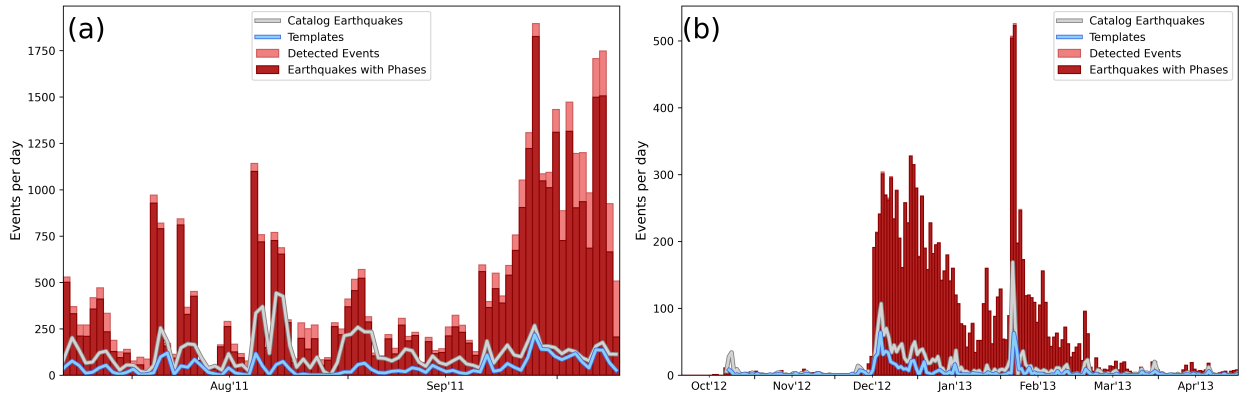


**Figure 3.** Evolution of the number of the events comparing the results automatically obtained (bars) with manual analysis (lines) for El Hierro (a) and Torreperogil (b). The pink bars represents the total number of detected events by our algorithm. Red bars represents the number of confirmed earthquakes detected. Gray line is the number of earthquakes in the IGN catalog and the blue line is the number of templates selected for our study

308 P-wave was not picked in the template, segmentation is done 5 seconds before the S-wave and 2  
 309 seconds after.

310 Furthermore, detections have been segmented in a 20 seconds windows, at each station: 5  
 311 seconds before detection and 15 seconds after. We have selected this time length to prevent possible  
 312 errors in the detection time. These lack of accuracy can result due to the energy calculation is  
 313 averaged over 1 second windows overlapping 0.5 seconds, so that the temporal precision decreases.

314 Templates have been cross correlated over the detection windows. Those with a  $NCCC \geq 0.7$   
 315 have been used to obtain the P and S *Robust Phases*. Then, we proceeded with the *Fine Phases* cal-  
 316 culation, for those stations where we had successfully obtained *Robust Phases*. The time windows  
 317 selected to determine the *Fine Phase* picking are: For templates, the P waves were segmented 1  
 318 second before and after the arrival and the S-wave, were segmented 1.5 seconds before and 1 sec-  
 319 ond after. Moreover, the traces with *Robust Phases* were segmented as it follows: 1 second before  
 320 the P *Robust Phase* and 1.5 seconds after and 1 second before the S *Robust Phase* and 2.5 seconds  
 321 after. These phases are cross correlated with the templates and those that obtain a  $NCCC \geq 0.8$  are  
 322 used to calculate the *Fine Phases*.

323 After the phase picking step, we have confirmed as real earthquakes 35 040 detections which  
 324 had, at least, a single successful correlation in one station (Figure 3a, red bars). The number of

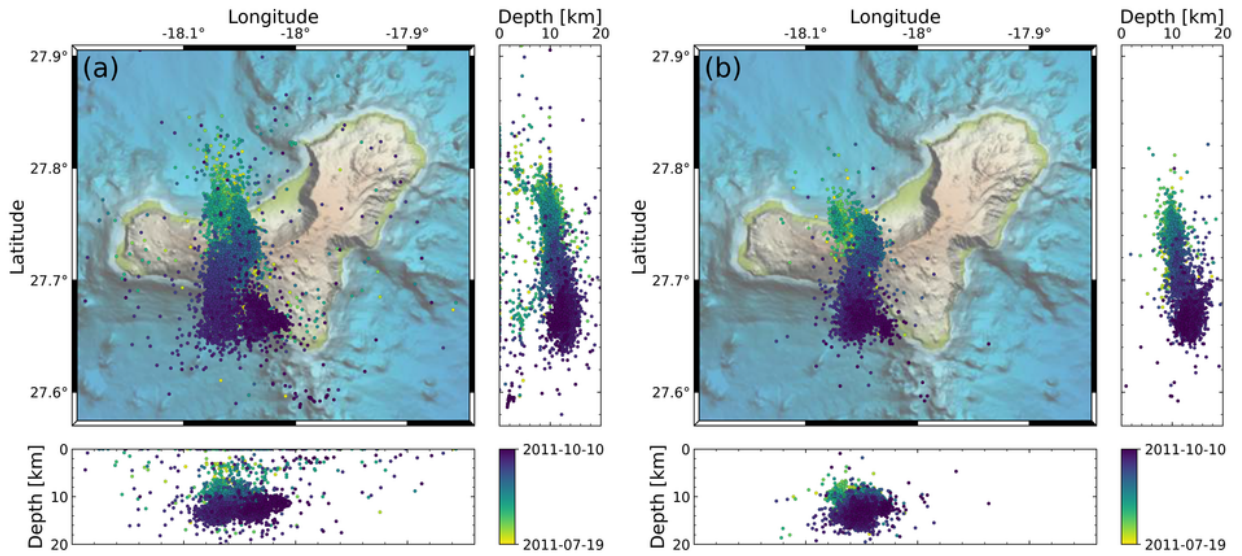


**Figure 4.** New seismic catalog for El Hierro: (a) Hypoellipse solutions. Panels show horizontal distribution and vertical projections in latitude and longitude. (b) *Master-Cluster* solutions. The color distribution indicates the time evolution, from 19<sup>th</sup> of July (yellow) to 10<sup>th</sup> of October (dark purple)

325 earthquakes confirmed in three or more stations is 29 836, which corresponds to the 85% of the  
 326 confirmed events. Comparing the number of phases obtained by phase picking and the manually  
 327 picked phases in the IGN catalog, our algorithm obtains 174 440 P phases and 174 780 S phases  
 328 versus the 22 423 P phases and 22 919 S phases of the IGN catalog, which means an increase in  
 329 a factor of 7.6 in the number of seismic phases. Moreover, phase classification has been settled  
 330 in terms of the phase quality (Sec. 2.2), separating the best quality phases (*Fine Phases*) from the  
 331 rest of the others (*Robust Phases*). When applying the cross-correlation method, the 30% of the P  
 332 arrivals and the 80% of the S arrivals were classified as *Fine Phases*.

333 Earthquakes with phases in three or more stations have been located with Hypoellipse (Fig.  
 334 4a). The resulting hypocentral locations obtained with our algorithm follow the same spatial dis-  
 335 tribution as in the IGN catalog (Fig. 1c). The increase with respect to the number of templates used  
 336 was a factor 8.2, while this factor is 2.9 with respect to the complete IGN catalog (Table 2).

337 Table 2 summarizes the results obtained for this seismic swarm. The 82% of the templates  
 338 used for the phase picking have been correctly retrieved and located using the phases obtained  
 339 automatically. Moreover, the 66% of the earthquakes from the IGN catalog which were non-used

340 as templates (magnitude  $mLg < 1.5$ ) have also been extracted from the continuous waveform and  
 341 has been located.

342 In the other hand, the events have been located by means of the *Master-Cluster* method, as  
 343 defined in Eq. 7, combined with the bootstrap method. The number of earthquakes located by  
 344 *Master-Cluster* method ascends to 21 086, which is an increment in a factor 2.1 larger than the  
 345 IGN catalog and a factor 5.9 larger than the number of earthquakes used as templates. *Master-*  
 346 *Cluster* solutions (Fig. 4b) define a more constrained and better defined structure than the previous  
 347 IGN catalog (Figure 1c). As it was expected, this results are more similar to those obtained by  
 348 HypoDD (Figure 1d).

349 In order to have a good approximation of the error intervals associated to our solutions, the  
 350 bootstrap method has been applied. Using the time residuals from Eq. 7 we have resampled 100  
 351 times the solution. Subsequently, each coordinate is taken as the median value of the resampling  
 352 and the error is estimated as the robust median of the resampling set. The latitude, longitude and  
 353 depth median for *Master-Cluster* are 121, 60, 93 meters, which are much lower in respect to  
 354 Hypoellipse errors 420, 1080, 860 meters.

## 355 4.2 Torreperogil

356 For the seismic swarm of Torreperogil, the analysis has followed the same schedule as in the pre-  
 357 vious dataset. The detector have been calibrated using three hours of data: the first two hours to  
 358 obtain the optimal parameter combinations and a third one to test the resulting parameter combi-  
 359 nation. The reference hours showed value of  $R = 0.62$  and  $F_1 = 0.77$  and the test hour showed a  
 360  $R = 0.69$  and  $F_1 = 0.81$ . The best parameter combination for our detector in this seismic swarm  
 361 uses a 6-13 Hz bandpass filter, 5 and 16 s for STA and LTA time window respectively and a 2.6  
 362 threshold to trigger the detector, and leads to a result of 12 006 potential events (pink bar in Fig.  
 363 3b). During the same period, 20<sup>th</sup> October 2012 and 1<sup>st</sup> May 2013, the IGN catalog includes 2 100  
 364 earthquakes registered in the same area (grey line in Fig. 3b).

365 The seismic network used in Torreperogil crisis covers from local distances (4-50 km) to re-  
 366 gional distances (80-140 km), (Fig. 2a, 2d). Therefore, we have adapted the template time lengths

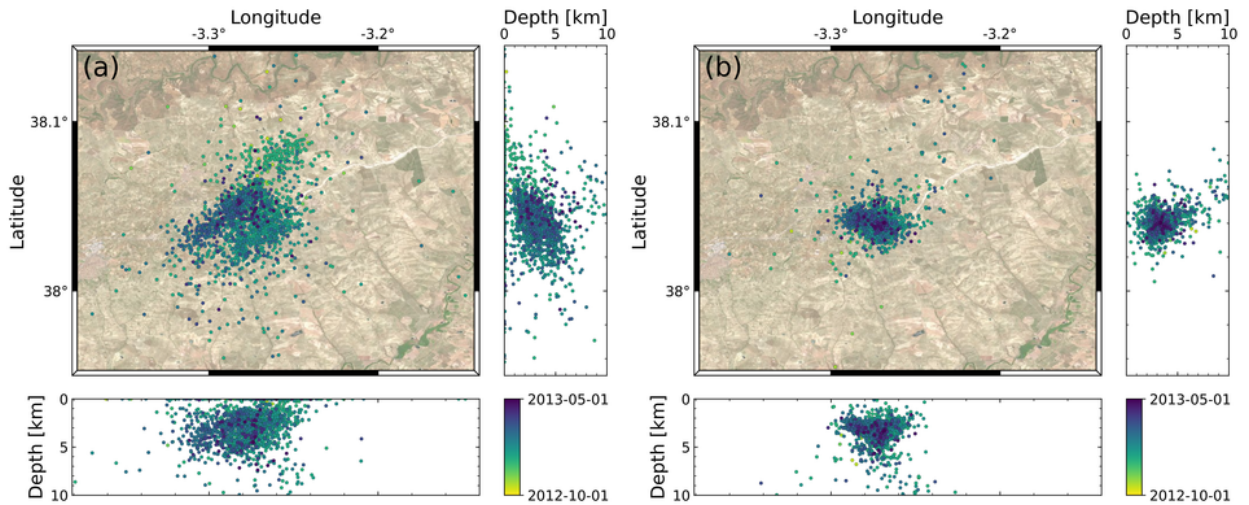


**Figure 5.** New seismic catalog for Torreperogil: (a) Hypoellipse solutions. Panels show horizontal distribution and vertical projections in latitude and longitude. (b) *Master-Cluster* solutions. Color distribution indicate the time evolution, from 1<sup>st</sup> of October of 2012 (yellow) to 1<sup>st</sup> of May of 2013 (dark purple).

367 to each station. These lengths were segmented from 3 seconds before P wave arrival to  $t_s - t_p + 3$   
 368 seconds after the P wave arrival. If there is no P wave picked, templates were segmented from  
 369  $t_s - t_p - 3$  seconds before the S arrival and 5 seconds after.

370 For local stations (4-50 km), the *Robust Phase* picking is calculated by a full wave cross cor-  
 371 relation around the detection time, 5 seconds before the detection and 15 seconds afterwards.  
 372 Subsequently, the *Fine Phase* picking was developed as it was introduced in Sec. 2.2; P wave tem-  
 373 plates were segmented from 1 second before to 1 second after the time arrival and the S wave from  
 374 1 second before to 2 seconds after the S-wave arrival. The detected events were cropped 1 second  
 375 before the P *Robust Phase* and 1.5 seconds after, and S *Robust Phase* from 1 second before to 2.5  
 376 seconds after.

377 For regional stations (80-140 km), we have extracted from the templates the P and S waves  
 378 and correlated them around the theoretical arrivals. At each station, the time window lengths to  
 379 correlate the templates with the detections depend on the time difference between the P and S  
 380 wave arrival. This dependence with  $t_S - t_P$  has been introduced to take into account the possible  
 381 error made in theoretical phase arrival determination. For the P-wave this window had a length of

382  $1/3(t_S - t_P)$  and for the S-wave  $3/5(t_S - t_P)$ . If *Robust Phases* were obtained, the *Fine Phases*  
383 are calculated following the same methodology as for the local stations.

384 The phase picking resulted a total of 11 885 confirmed events (red bar in Fig. 3b). From them,  
385 11 827 include detections in three or more stations and 10 899 in at least 4 stations, being, respec-  
386 tively the 99% and 90% of the all detected earthquakes. Comparing the number of P and S waves  
387 obtained versus the template phases there has been an increment in a factor 10: From 76 868 and  
388 82 807 P and S waves with cross correlation, to 7 792 P and 7 406 S template waveforms. Using a  
389 threshold of 0.7 for the cross correlation in *Robust Phases* and 0.8 for *Fine Phases*, we found that  
390 52.1% of the P waves and 69.6% of the S waves were classified as *Fine Phases*.

391 The IGN catalog has 796 locatable earthquakes with a magnitude (mbLg) higher or equal to  
392 1.5, which have been used as templates, and 1 324 locatable earthquakes with lower magnitude.  
393 Our method have picked automatically the 92% of the templates and the 87% of the low magnitude  
394 earthquakes. Altogether, 10 008 earthquakes have been successfully located applying Hypoellipse  
395 (Figure 5a) algorithm to the cross correlated phases, which means 4.7 more earthquakes than  
396 IGN catalog currently have (Figure 2c). Median errors associated to hypoellipse solutions are for  
397 latitude, longitude and depth 360, 790, 2490 meters respectively.

398 As in El Hierro, the *Master-Cluster* algorithm has been applied using bootstrapping (Figure  
399 5b). This method has been applied, resampling the solution 100 times. As a results, the method  
400 have located 8 460 earthquakes. From those, the 85% of the IGN catalog, the 86% of the templates  
401 and 85% of the non used templates (mbLg<1.5). This number is a factor 4 higher than the number  
402 of registered earthquakes in the IGN catalog for the same period and 10.6 times of the 796 earth-  
403 quakes used as templates. *Master-Cluster* have median errors for latitude longitude and depth 14,  
404 85, 100 meters respectively.

## 405 5 DISCUSSION

406 The application of the proposed methodology to the seismic series of El Hierro and Torreperogil  
407 has significantly increased the number of analyzed earthquakes for both swarms. After consid-



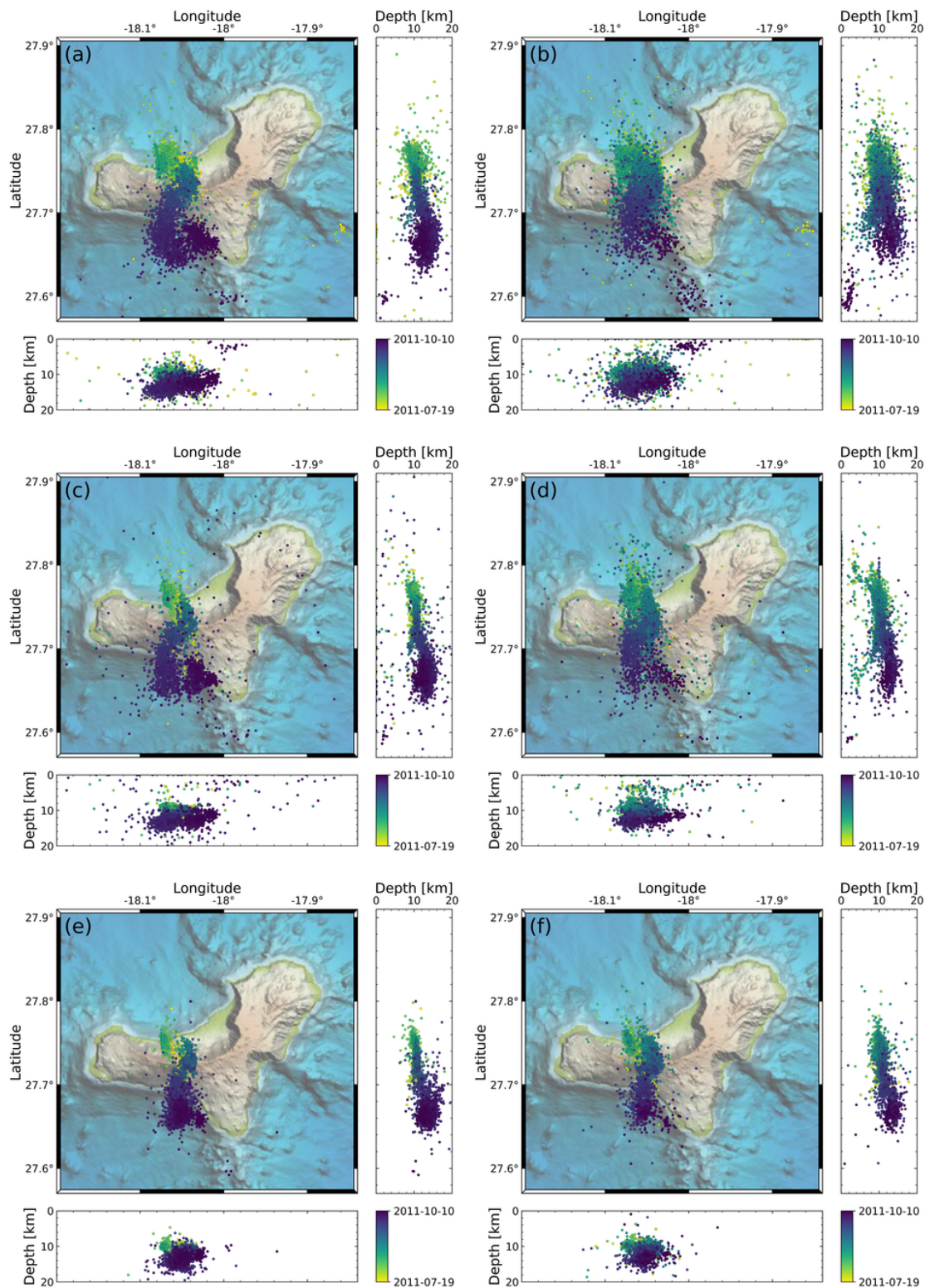


**Figure 6.** Results of the automatic system for the El Hierro IGN catalog events separated in templates ( $m \geq 1.5$ ; left panels) and low magnitude earthquakes not used as templates ( $m < 1.5$ ; right panels). From top to bottom we show locations by Hypoellipse from manually picked phases (a, b), locations by Hypoellipse using automatic picked phases (c, d) and locations from *Master-Cluster* method.

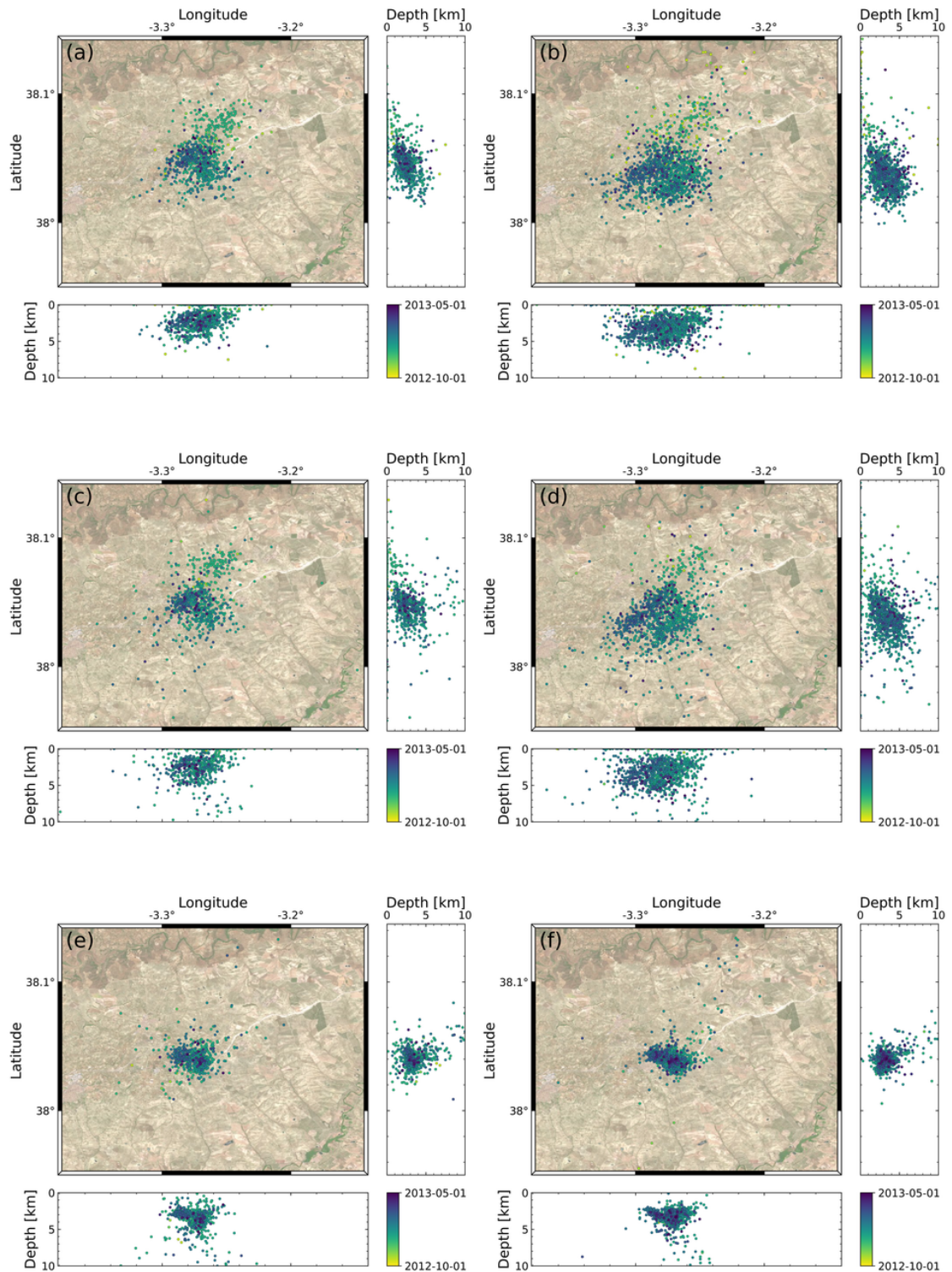


**Figure 7.** Results of the automatic system for the Torreperogil IGN catalog events separated in templates ( $m \geq 1.5$ ; left panels) and low magnitude earthquakes not used as templates ( $m < 1.5$ ; right panels). From top to bottom we show locations by Hypoellipse from manually picked phases (a, b), locations by Hypoellipse using automatic picked phases (c, d) and locations from *Master-Cluster* method.

**Table 2.** Number of earthquakes for different subsets including the IGN Catalog and New Catalog obtained with our algorithm for El Hierro and Torreperogil datasets. New Catalog is splitted in Detections (potential events confirmed), Locations (events from Detections located with Hypoellipse) and *Master-Cluster* (events relocated with *Master-Cluster*). Numbers are given for results on templates (IGN Catalog,  $m \geq 1.5$ ), low-magnitude earthquakes from original catalog (IGN Catalog,  $m < 1.5$ ) and events added to the new catalog (New Events)

Data Set	Classification	IGN Catalog		New Catalog	
			Detections	Locations	<i>Master-Cluster</i>
El Hierro	IGN Catalog ( $m \geq 1.5$ )	3 601	2 939	2 936	2 930
	IGN Catalog ( $m < 1.5$ )	6 377	4 223	4 214	3 999
	New Events	-	28 138	19 601	14 157
	Total	9 978	35 300	26 751	21 086
Torreperogil	IGN Catalog ( $m \geq 1.5$ )	796	752	733	687
	IGN Catalog ( $m < 1.5$ )	1 324	1 170	1 159	1 123
	New Events	-	9 880	8 116	6 650
	Total	2 120	11 802	10 008	8 460

408 ering 3 601 templates for El Hierro and 796 for Torreperogil, the resulting number of potential  
409 earthquakes is at least a factor 11 higher than the number of templates.

410 The cross-correlation phase picking has allowed us to discriminate between earthquakes and  
411 false positive detections. In both datasets, the difference between real earthquakes in at least one  
412 station and false detections is not very significant: in El Hierro 13% of the detections are false  
413 positives and 2% in Torreperogil. Hence, we consider the calibrations of the detector good enough  
414 for the automatic algorithm to work without further supervision.

415 We have assumed that the templates we have selected from the seismic catalog are representa-  
416 tive of the activity and reflect all the possible families of earthquakes in these series. Otherwise, it  
417 remains the possibility that some of the events we have labelled as false positives are earthquakes  
418 for which there is no template in our catalogues. This situation would be more likely to occur in the  
419 case of El Hierro crisis, where the waveform of the families is evolving since the seismicity was as-  
420 sociated with magma migration and a larger number of families are involved (Domínguez Cerdeña  
421 et al., 2014). For this case, a manual review has been made in case it was a systematic error or a



422 family of earthquakes for which there was no record in the selected templates. We have found that  
423 mostly, the earthquakes that fail to be analyzed are at the end of the series (Fig. 3a). Nevertheless,  
424 the apparent false detections are a small percentage of the total events. These numbers are reason-  
425 able ratios, considering the variability of the seismic network (Figs. 2b 1b), the earthquakes with a  
426 low signal to noise ratio and the limitations of the method itself, especially during the first period  
427 of the swarms when a low number of stations were available.

428 Locations obtained by applying Hypoellipse (Fig. 4a and Fig. 5b) are consistent with the previ-  
429 ous locations obtained by manual analysis (Fig. 1c and Fig 2c) in both data sets. These solutions are  
430 consistent with the results shown in previous works (Cantavella et al. 2013; Domínguez Cerdeña  
431 et al. 2014) with similar epicentral distributions, but with larger scatter. This apparent low qual-  
432 ity of the locations is produced by the large number of earthquakes with lower magnitude picked  
433 automatically.

434 The *Master-Cluster* event methodology shows a substantial improvement of the earthquake  
435 locations in El Hierro (Fig. 4b), despite decreasing the number of converging earthquakes by 26%  
436 with respect to those located with Hypoellipse (Fig. 4a). In the case of Torreperogil, the earth-  
437 quakes located by Hypoellipse show a similar distribution (Fig. 5a) as the original IGN catalog  
438 (Fig. 2c) while the *Master-Cluster* method shows an important improvement in the hypocentral  
439 location (Fig. 5b), but with larger dispersion than El Hierro solutions. This difference is probably  
440 related to the different path of the traces, the scenario of El Hierro deals with rays coming from  
441 a source at 12 km depth recorded at local stations, most of the rays arrive almost vertically in the  
442 stations and show in most of the cases impulsive P and S arrivals. In Torreperogil, sources are  
443 shallower and some of the stations used are placed at regional scales, more refracted and reflected  
444 waves are produced in the upper crust and also rays are more likely to be affected by other phe-  
445 nomena as scattering. In consequence, seismic phases are more emergent and more difficult to be  
446 identified. Also, the assignment of phases to an event may be poorly done for stations at large  
447 distances due to the large width of windows chosen for phase picking by cross-correlation. Addi-  
448 tionally, the filters used for cross-correlation at stations at local distances respect to the regional  
449 ones are not optimal for the identification of seismic phases. Finally, the velocity model used for

450 both datasets may increase the uncertainties in the location since it may not be the optimal for  
451 these areas, especially for stations at local distances, as they may have a worse determination of  
452 the hypocentre. However, for this work, we have not discussed the ground velocity models appli-  
453 cable to both areas. Despite the existence of a local velocity model for Torreperogil (Serrano et al.  
454 2015) it was impossible to apply it with regional and local stations at the same time. There is also  
455 a 3D model for El Hierro island (García-Yeguas et al. 2014), however, the model is not published  
456 and it is not possible to apply it to HypoDD or Hypoellipse algorithm. Therefore, we have used  
457 the IGN generic velocity model for the whole Iberian Peninsula or the Canary Islands. A more de-  
458 tailed ground model for the stations at local distances can give a more detailed model for the local  
459 distances. Consequently, the possibility of studying the influence of the different earth models on  
460 the location of the series remains open.

461 In order to perform a proper analysis of the capabilities of the method, we have carefully an-  
462 alyzed the results obtained only for IGN catalog events, including low magnitude earthquakes  
463 ( $m_b L_g < 1.5$ ) not used as templates (Figs. 6, 7). In both cases most of the earthquakes were auto-  
464 matically located even improving the result from the manual catalog. For the case of El Hierro,  
465 there is a substantial improvement in the locations obtained with Hypoellipse by our automatic  
466 methodology (Fig. 6d), with respect to the manually analyzed seismicity (Fig. 6b). This is a con-  
467 sequence of manual picking for low magnitude earthquakes, usually biased due to the low signal-  
468 to-noise ratio, implying higher residuals due to the difficult to clearly identify the arrival of the  
469 seismic phases. This result is the most remarkable when it comes to possible implementation in  
470 real-time systems since these earthquakes are usually the most difficult to manually analyze.

471 For the case of Torreperogil we found similar Hypoellipse locations for the low magnitude  
472 seismicity manually (Fig. 7b) or automatically picked (Fig. 7d). Despite there is not an improve-  
473 ment in the locations the number of automatic analyzed earthquakes is indeed a major advance.  
474 The comparison described above for both swarms is independent of the availability of relocated  
475 templates which may take advantage of reanalyzed events that may not be accessible to the au-  
476 tomatic method in case of a real time application of the method. For both cases there is a clear  
477 improvement in the locations when we compare manually picked earthquakes with those obtained

478 by the *Master-Cluster* method (Figs 6f and 7f) with almost no loss on number of events due to  
479 missconvergence (Table 2).

480 A further test on our methodology is its capability to recover automatically the templates with  
481 the better possible quality. The results are in both cases very similar as for the low magnitude  
482 events. In the case of El Hierro there is an important improvement between manually picked (Fig.  
483 6a) and automatically (Fig. 6c) located events with Hypoellipse. The *Master-Cluster* result (Fig.  
484 6e) is remarkable with a similar result as the actual relocated events (Fig. 1d). In the case of  
485 Torreperogil the result is very similar for manually picked (Fig. 7a) and automatically (Fig. 7c)  
486 located events with Hypoellipse. The distribution of the seismicity obtained with *Master-Cluster*  
487 (Fig. 7e) shows much more clustering than the manually picked but is not as good result as that  
488 obtained directly by relocation (Fig. 2d).

489 In El Hierro, the phase picking and localization consumes a total of 20 seconds per event,  
490 while it was 12 seconds for Torreperogil events. The average detection time per hour is 10 seconds  
491 for both crises. Using an Intel (R) core (TM) i7-8700 CPU 3.200 GHz, 6 cores-12 threads, the  
492 total elapsed time for El Hierro, 3 months of data in 11 stations have been 84.6 hours, while, in  
493 Torreperogil, 13 stations with 7 months of data the computer spent 61.2 hours. This time difference  
494 is explained by the difference in the number of earthquakes detected during the seismic crises.  
495 Therefore, the automatic method seems to reliably reproduce the manual analysis in a considerably  
496 shorter time.

## 497 **6 CONCLUSIONS**

498 We have implemented an automatic detection and location method for seismic swarms that im-  
499 proves the results of manual analysis and can save a large amount of time in any seismological  
500 observatory. In addition to improved catalog localization, the resulting catalog is greatly expanded,  
501 which can improve the completeness of the seismic catalog. This is essential to provide more de-  
502 tailed information on processes, whether they are purely tectonic seismic series or those related to  
503 volcanic activity, which can produce a substantial improvement in the forecast of volcanic erup-  
504 tions. This work also presents a new technique for relocation, *Master-Cluster*, which takes

505 advantage of two well known techniques, the master event and the double differences. This tech-  
506 nique may be used in our automatic system to enhance the seismic catalogs, especially when a  
507 relocated catalog is available.

508 By using a small number of earthquakes as characteristic templates of both swarms, we have  
509 extended the number of earthquakes analysed with short computation times. In El Hierro, with  
510 3 601 relocated and manually picked templates, more than 35 000 earthquakes have been con-  
511 firmed and more than 27 000 earthquakes have been located with Hypoellipse and 22 000 with  
512 the *Master-Cluster* method. In Torreperogil, with 796 relocated and manually picked templates,  
513 more than 11 800 earthquakes have been confirmed, of which almost 10 000 have been located  
514 by Hypoellipse and approximately 8 000 by the *Master-Cluster* method. Both results show less  
515 scatter in the hypocentral distributions and are able to reproduce more accurately the catalogue  
516 earthquakes that have not been used as templates.

517 Despite is not a purely automatic system, it is still to be analyze the needed number of templates  
518 to produce a substantial improvement. Moreover, since the templates are the larger earthquakes  
519 (in our work  $m \geq 1.5$ ) this template catalog can be obtained by other automatic methodologies  
520 which may work well by high SNR events. The only use of the automatic phases obtained from  
521 the correlation with templates of the original seismic catalog has given an improved new catalog  
522 with similar or even better location. This fact has been proved by the tests performed with the  
523 low magnitude events from the original catalog. The application of the *Master-Cluster* method to  
524 these results improves substantially the hypocentral locations thanks to the use of a better relocated  
525 catalog of templates. However, this is not essential to be used in an hypothetical real time automatic  
526 system, and can be applied at any post-process analysis when a relocated catalog of templates is  
527 available.

## 528 **7 ACKNOWLEDGMENTS**

529 The authors would like to thank Jaime Barco, Resurrección Antón and Juan Vicente Cantavella for  
530 their comments, clarifications and access to the Torreperogil crisis data (2012-2013). They would  
531 also like to thank the 24-hour shift of the Spanish National Seismic Network (IGN) and the Vol-

cano Monitoring Group (IGN) who did a titanic task in the manual analysis of the earthquakes preceding El Hierro eruption (2011). This research was partially supported by the Spanish National Geographic Institute of the Spanish Ministry of Transport, Mobility and Urban Agenda and through project CGL2014-53044-R of the Spanish Ministry of Economy and Competitiveness.

## 8 DATA AVAILABILITY

The data used in this article have been obtained from the continuous recording network of seismic stations of the Spanish National Geographic Institute. The seismic data belong to the IGN and can be accessed by request. The catalogues used can be exploited from the IGN's website (<https://www.ign.es/web/ign/portal>).

## REFERENCES

- Allen, R., 1982. Automatic phase pickers: Their present use and future prospects, *Bulletin of the Seismological Society of America*, **72**(6B), S225–S242.
- Baer, M. & Kradolfer, U., 1987. An automatic phase picker for local and teleseismic events, *Bulletin of the Seismological Society of America*, **77**(4), 1437–1445.
- Beaucé, E., Frank, W. B., & Romanenko, A., 2017. Fast Matched Filter (FMF): An Efficient Seismic Matched-Filter Search for Both CPU and GPU Architectures, *Seismological Research Letters*, **89**(1), 165–172.
- Bent, A. L., Cassidy, J., Prépetit, C., Lamontagne, M., & Ulysse, S., 2018. Real-Time Seismic Monitoring in Haiti and Some Applications, *Seismological Research Letters*, **89**(2A), 407–415.
- Benz, H., 2017. Building a National Seismic Monitoring Center: NEIC from 2000 to the Present, *Seismological Research Letters*, **88**(2A), 265–269.
- Beyreuther, M., Barsch, R., Krischer, L., Megies, T., Behr, Y., & Wassermann, J., 2010. ObsPy: A Python Toolbox for Seismology, *Seismological Research Letters*, **81**(3), 530–533.
- Bianchi, M. B., Assumpção, M., Rocha, M. P., Carvalho, J. M., Azevedo, P. A., Fontes, S. L., Dias, F. L., Ferreira, J. M., Nascimento, A. F., Ferreira, M. V., & Costa, I. S. L., 2018. The Brazilian Seismographic Network (RSBR): Improving Seismic Monitoring in Brazil, *Seismological Research Letters*, **89**(2A), 452–457.
- Cantavella, J., Morales, J., & Martinez-Solares, J., 2013. La serie sísmica de la comarca de La Loma (Jaén). Antecedentes, distribución temporal, localización y mecanismo focal, Jaen. Informe del grupo de

- 561 trabajo interinstitucional sobre la actividad sísmica en la comarca de la loma (Jaen), Tech. rep., Ministerio  
562 de Fomento, Madrid.
- 563 Carmona, E., Almendros, J., Peña, J. A., & Ibáñez, J. M., 2010. Characterization of fracture systems using  
564 precise array locations of earthquake multiplets: An example at deception island volcano, antarctica,  
565 *Journal of Geophysical Research: Solid Earth*, **115**(B6).
- 566 Cesca, S. & Grigoli, F., 2015. Chapter two - full waveform seismological advances for microseismic  
567 monitoring, in *Advances in Geophysics*, vol. 56, pp. 169–228, ed. Dmowska, R., Elsevier.
- 568 Chamberlain, C. J., Hopp, C. J., Boese, C. M., Warren-Smith, E., Chambers, D., Chu, S. X., Michailos, K.,  
569 & Townend, J., 2017. EQcorrscan: Repeating and Near-Repeating Earthquake Detection and Analysis in  
570 Python, *Seismological Research Letters*, **89**(1), 173–181.
- 571 Chamberlain, C. J., Townend, J., & Gerstenberger, M. C., 2020. RT-EQcorrscan: Near-Real-Time  
572 Matched-Filtering for Rapid Development of Dense Earthquake Catalogs, *Seismological Research Let-  
573 ters*, **91**(6), 3574–3584.
- 574 Domínguez Cerdeña, I., del Fresno, C., & Rivera, L., 2011. New insight on the increasing seismicity  
575 during tenerife’s 2004 volcanic reactivation, *Journal of Volcanology and Geothermal Research*, **206**(1),  
576 15 – 29.
- 577 Domínguez Cerdeña, I., del Fresno, C., & Gomis Moreno, A., 2014. Seismicity Patterns Prior to the 2011  
578 El Hierro Eruption. Short Note, *Bulletin of the Seismological Society of America*, **104**(1), 567–575.
- 579 Dondin, F. J.-Y., Lynch, L., Ramsingh, C., Ryan, G. A., Papadopoulos, I., Rueppel, D., Joseph, E. P.,  
580 Latchman, J. L., Robertson, R. E. A., Nath, N., Mathura, R., Balchan, A., George, S., Juman, I., Madoo,  
581 F., Manette, G., & Ramsingh, H., 2019. The university of the west indies-seismic research centre volcano  
582 monitoring network: Evolution since 1953 and challenges in maintaining a state-of-the-art network in a  
583 small island economy, *Geosciences*, **9**(2).
- 584 Efron, B., 1982. *The Jackknife, the bootstrap and other resampling plans*, no. 38 in Regional Conference  
585 Series in applied mathematics, Society for Industrial and applied mathematics, Philadelphia, Pa.
- 586 García-Yeguas, A., Ibáñez, J. M., Koulakov, I., Jakovlev, A., Romero-Ruiz, M. C., & Prudencio, J., 2014.  
587 Seismic tomography model reveals mantle magma sources of recent volcanic activity at El Hierro Island  
588 (Canary Islands, Spain), *Geophysical Journal International*, **199**(3), 1739–1750.
- 589 González, Á., 2017. The spanish national earthquake catalogue: Evolution, precision and completeness,  
590 *Journal of Seismology*, **21**(3), 435–471.
- 591 Got, J.-L., Fréchet, J., & Klein, F. W., 1994. Deep fault plane geometry inferred from multiplet relative  
592 relocation beneath the south flank of kilauea, *Journal of Geophysical Research: Solid Earth*, **99**(B8),  
593 15375–15386.
- 594 Grigoli, F., Cesca, S., Priolo, E., Rinaldi, A. P., Clinton, J. F., Stabile, T. A., Dost, B., Fernandez, M. G.,  
595 Wiemer, S., & Dahm, T., 2017. Current challenges in monitoring, discrimination, and management

- 596 of induced seismicity related to underground industrial activities: A european perspective, *Reviews of*  
597 *Geophysics*, **55**(2), 310–340.
- 598 Gutenberg, B. & Richter, C. F., 1944. Frequency of earthquakes in California\*, *Bulletin of the Seismolog-*  
599 *ical Society of America*, **34**(4), 185–188.
- 600 Harris, C. R., Millman, K. J., van der Walt, S. J., Gommers, R., Virtanen, P., Cournapeau, D., Wieser, E.,  
601 Taylor, J., Berg, S., Smith, N. J., Kern, R., Picus, M., Hoyer, S., van Kerkwijk, M. H., Brett, M., Haldane,  
602 A., del R'io, J. F., Wiebe, M., Peterson, P., G'erard-Marchant, P., Sheppard, K., Reddy, T., Weckesser, W.,  
603 Abbasi, H., Gohlke, C., & Oliphant, T. E., 2020. Array programming with NumPy, *Nature*, **585**(7825),  
604 357–362.
- 605 Hesterberg, T., Monaghan, S., Moore, D., Clipson, A., Epstein, R., Freeman, W., & York, C., 2005. Boot-  
606 strap methods and permutation tests, *Introduction to the Practice of Statistics*, **14**.
- 607 Instituto Geografico Nacional, Spain, 1999. Spanish digital seismic network.
- 608 Ito, A., 1985. High resolution relative hypocenters of similar earthquakes by cross-spectral analysis  
609 method, *Journal of Physics of the Earth*, **33**(4), 279–294.
- 610 Jourdan, D. B. & de Weck, O. L., 2004. Layout optimization for a wireless sensor network using a multi-  
611 objective genetic algorithm, in *2004 IEEE 59th Vehicular Technology Conference. VTC 2004-Spring*  
612 *(IEEE Cat. No.04CH37514)*, vol. 5, pp. 2466–2470 Vol.5.
- 613 Journeau, C., Shapiro, N. M., Seydoux, L., Soubestre, J., Ferrazzini, V., & Peltier, A., 2020. Detection,  
614 classification, and location of seismovolcanic signals with multi-component seismic data, example from  
615 the Piton de la Fournaise volcano (La Réunion, France), *Journal of Geophysical Research : Solid Earth*.
- 616 Kao, H. & Shan, S., 2007. Rapid identification of earthquake rupture plane using Source-Scanning Algo-  
617 rithm, *Geophysical Journal International*, **168**(3), 1011–1020.
- 618 Kao, H. & Shan, S.-J., 2004. The Source-Scanning Algorithm: mapping the distribution of seismic sources  
619 in time and space, *Geophysical Journal International*, **157**(2), 589–594.
- 620 Küperkoch, L., Meier, T., Lee, J., Friederich, W., & Working Group, E., 2010. Automated determination  
621 of p-phase arrival times at regional and local distances using higher order statistics, *Geophysical Journal*  
622 *International*, **181**(2), 1159–1170.
- 623 Lahr, J., Chouet, B., Stephens, C., Power, J., & Page, R., 1994. Earthquake classification, location, and  
624 error analysis in a volcanic environment: implications for the magmatic system of the 1989–1990 erup-  
625 tions at redoubt volcano, alaska, *Journal of Volcanology and Geothermal Research*, **62**(1), 137 – 151,  
626 The 1989-1990 Eruptions of Redoubt Volcano, Alaska.
- 627 Lahr, J. C., 1999. HYPOELLIPSE: a computer program for determining local earthquake hypocentral  
628 parameters, magnitude, and first-motion pattern, *U.S. Geological Survey Open-File Report*, **99**(23), 119.
- 629 Leys, C., Ley, C., Klein, O., Bernard, P., & Licata, L., 2013. Detecting outliers: Do not use standard  
630 deviation around the mean, use absolute deviation around the median, *Journal of Experimental Social*

- 631 *Psychology*, **49**(4), 764–766.
- 632 Liu, M., Zhang, M., Zhu, W., Ellsworth, W. L., & Li, H., 2020. Rapid characterization of the July 2019  
633 ridgecrest, California, earthquake sequence from raw seismic data using machine-learning phase picker,  
634 *Geophysical Research Letters*, **47**(4), e2019GL086189, e2019GL086189 2019GL086189.
- 635 Lopes Pereira, R., Trindade, J., Gonçalves, F., Suresh, L., Barbosa, D., & Vazão, T., 2014. A wireless  
636 sensor network for monitoring volcano-seismic signals, *Natural Hazards and Earth System Sciences*,  
637 **14**(12), 3123–3142.
- 638 López, C., Blanco, M. J., Abella, R., Brenes, B., Cabrera Rodríguez, V. M., Casas, B., Domínguez Cerdeña,  
639 I., Felpeto, A., de Villalta, M. F., del Fresno, C., García, O., García-Arias, M. J., García-Cañada, L.,  
640 Gomis Moreno, A., González-Alonso, E., Guzmán Pérez, J., Iribarren, I., López-Díaz, R., Luengo-Oroz,  
641 N., Meletlidis, S., Moreno, M., Moure, D., de Pablo, J. P., Rodero, C., Romero, E., Sainz-Maza, S.,  
642 Sentre Domingo, M. A., Torres, P. A., Trigo, P., & Villasante-Marcos, V., 2012. Monitoring the volcanic  
643 unrest of el hierro (canary islands) before the onset of the 2011–2012 submarine eruption, *Geophysical  
644 Research Letters*, **39**(13).
- 645 Mammen, E., 1992. *When Does Bootstrap Work?*, Springer New York.
- 646 Maronna, R., 2011. Robust statistical methods, in *International Encyclopedia of Statistical Science*, pp.  
647 1244–1248, Springer Berlin Heidelberg.
- 648 McKerns, M. M., Strand, L., Sullivan, T., Fang, A., & Aivazis, M. A. G., 2012. Building a framework for  
649 predictive science.
- 650 Meletlidis, S., Roberto, A. D., Cerdeña, I. D., Pompilio, M., García-Cañada, L., Bertagnini, A., Benito-  
651 Saz, M. A., Carlo, P. D., & Aparicio, S. S.-M., 2015. New insight into the 2011-2012 unrest and eruption  
652 of el hierro island (canary islands) based on integrated geophysical, geodetical and petrological data,  
653 *Annals of Geophysics*, **58**(5), 0546.
- 654 Mignan, A. & Chouliaras, G., 2014. Fifty Years of Seismic Network Performance in Greece (1964–2013):  
655 Spatiotemporal Evolution of the Completeness Magnitude, *Seismological Research Letters*, **85**(3), 657–  
656 667.
- 657 Murphy, K. P., 2012. *Machine learning: a probabilistic perspective*, MIT press.
- 658 Okada, H., Watanabe, H., Yamashita, H., & Yokoyama, I., 1981. Seismological significance of the  
659 1977–1978 eruptions and the magma intrusion process of usu volcano, hokkaido, *Journal of Volcanology  
660 and Geothermal Research*, **9**(4), 311 – 334.
- 661 Pedrera, A., Ruiz-Constán, A., Marín-Lechado, C., Galindo-Zaldívar, J., González, A., & Peláez, J. A.,  
662 2013. Seismic transpressive basement faults and monocline development in a foreland basin (eastern  
663 guadalquivir, se Spain), *Tectonics*, **32**(6), 1571–1586.
- 664 Peláez, J. A., Francisco J., G.-T., Mario, S.-G., Carlos, S. d. G., Fernando, P.-V., & Jesús, H.-R., 2013. La  
665 serie sísmica de torreperogil-sabiote (jaén), *Enseñanza de las Ciencias de la Tierra*, **21**(3), 336.



- 666 Perol, T., Gharbi, M., & Denolle, M., 2018. Convolutional neural network for earthquake detection and  
667 location, *Science Advances*, **4**(2).
- 668 Sainz-Maza Aparicio, S., Arnosó Sampedro, J., Gonzalez Montesinos, F., & Martí Molist, J., 2014. Vol-  
669 canic signatures in time gravity variations during the volcanic unrest on el hierro (canary islands), *Journal*  
670 *of Geophysical Research: Solid Earth*, **119**(6), 5033–5051.
- 671 Saragiotis, C. D., Hadjileontiadis, L. J., & Panas, S. M., 2002. Pai-s/k: A robust automatic seismic p phase  
672 arrival identification scheme, *IEEE Transactions on Geoscience and Remote Sensing*, **40**(6), 1395–1404.
- 673 Senobari, N. S., Funning, G. J., Keogh, E., Zhu, Y., Yeh, C.-C. M., Zimmerman, Z., & Mueen, A., 2019.  
674 Super-efficient cross-correlation (sec-c): A fast matched filtering code suitable for desktop computers,  
675 *Seismological Research Letters*, **90**(1), 322–334.
- 676 Serrano, I., Torcal, F., & Martín, J. B., 2015. “high resolution seismic imaging of an active fault in the  
677 eastern guadaluquivir basin (betic cordillera, southern spain)”, *Tectonophysics*, **660**, 79–91.
- 678 Stephens, C. & Chouet, B., 2001. Evolution of the december 14, 1989 precursory long-period event swarm  
679 at redoubt volcano, alaska, *Journal of Volcanology and Geothermal Research*, **109**(1-3), 133–148.
- 680 Sánchez-Gómez, M., Peláez, J., García-Tortosa, F., Valera, F., & Sanz de Galdeano, C., 2014. La serie  
681 sísmica de torreperogil (jaén, cuenca del guadaluquivir oriental): Evidencias de deformacion tectonica en  
682 el área epicentral, *Revista de la Sociedad Geológica de España*, **27**, 301–318.
- 683 Trugman, D. T. & Shearer, P. M., 2017. GrowClust: A Hierarchical Clustering Algorithm for Relative  
684 Earthquake Relocation, with Application to the Spanish Springs and Sheldon, Nevada, Earthquake Se-  
685 quences, *Seismological Research Letters*, **88**(2A), 379–391.
- 686 Umakoshi, K., Takamura, N., Shinzato, N., Uchida, K., Matsuwo, N., & Shimizu, H., 2008. Seismic-  
687 ity associated with the 1991–1995 dome growth at unzen volcano, japan, *Journal of Volcanology and*  
688 *Geothermal Research*, **175**(1), 91 – 99, Scientific drilling at Mount Unzen.
- 689 Virtanen, P., Gommers, R., Oliphant, T. E., Haberland, M., Reddy, T., Cournapeau, D., Burovski, E.,  
690 Peterson, P., Weckesser, W., Bright, J., van der Walt, S. J., Brett, M., Wilson, J., Millman, K. J., Mayorov,  
691 N., Nelson, A. R. J., Jones, E., Kern, R., Larson, E., Carey, C. J., Polat, Í., Feng, Y., Moore, E. W.,  
692 VanderPlas, J., Laxalde, D., Perktold, J., Cimrman, R., Henriksen, I., Quintero, E. A., Harris, C. R.,  
693 Archibald, A. M., Ribeiro, A. H., Pedregosa, F., van Mulbregt, P., & SciPy 1.0 Contributors, 2020. SciPy  
694 1.0: Fundamental Algorithms for Scientific Computing in Python, *Nature Methods*, **17**, 261–272.
- 695 Vuan, A., Sukan, M., Amati, G., & Kato, A., 2018. Improving the Detection of Low-Magnitude Seismic-  
696 ity Preceding the Mw 6.3 L’Aquila Earthquake: Development of a Scalable Code Based on the Cross  
697 Correlation of Template Earthquakes, *Bulletin of the Seismological Society of America*, **108**(1), 471–480.
- 698 Waldhauser, F. & Ellsworth, W. L., 2000. A Double-Difference Earthquake Location Algorithm: Method  
699 and Application to the Northern Hayward Fault, California, *Bulletin of the Seismological Society of*  
700 *America*, **90**(6), 1353–1368.

- 701 Werner-Allen, G., Dawson-Haggerty, S., & Welsh, M., 2008. Lance: Optimizing high-resolution signal  
702 collection in wireless sensor networks, in *Proceedings of the 6th ACM Conference on Embedded Network*  
703 *Sensor Systems*, SenSys '08, p. 169–182, Association for Computing Machinery, New York, NY, USA.
- 704 Yazdi, P., Hainzl, S., & Gaspar-Escribano, J. M., 2017. Statistical analysis of the 2012–2013 torreperogil–  
705 sabiote seismic series, spain, *Journal of Seismology*, **21**(4), 705–717.
- 706 Zhu, W. & Beroza, G. C., 2018. PhaseNet: a deep-neural-network-based seismic arrival-time picking  
707 method, *Geophysical Journal International*, **216**(1), 261–273.